Original Research Article

Measuring the fire growth potential of combustible solids using a cone calorimeter

Richard E Lyon (ID)

Date received: 20 March 2024; accepted: 5 June 2024

Abstract

The fire growth rate of interior linings, furnishings, and construction materials is measured in full-scale fire tests such as the ASTM E84 Steiner Tunnel, the ISO 9705 room fire, and a passenger aircraft fuselage as the flame-spread rate, time-to-flashover, or time to incapacitation, respectively. The results are used to indicate the level of passive fire protection afforded by the combustible material or product in the test without providing any insight into the burning process. These large-scale tests require many square meters of product, are very expensive to conduct, and can exhibit poor repeatability–making them unsuitable for product development, quality control, product surveillance, or regulatory compliance. For this reason, smaller (0.01 m^2) samples are tested in bench-scale fire calorimeters under controlled conditions, and these one-dimensional burning histories are correlated with the results of the two- and three-dimensional burning histories in full-scale fire tests by a variety of empirical and semi-empirical fire propagation indices, as well as analytic and computer models specific to the full-scale fire test. The approach described here defines the potential of a material to grow a fire in terms of cone calorimeter data obtained under standard conditions. The fire growth potential, λ (m^2/J), is the coupled process of surface flame spread and in-depth burning that is defined as the product of ignitability ($1/E_{ign}$) and combustibility ($\Delta Q/\Delta E$) obtained from a combustion energy diagram measured in a cone calorimeter at an external radiant energy flux $\dot{q}_{ext}$ (W/m^2) above the critical flux for burning, $\dot{q}_{burn}$. However, the potential for fire growth, $\lambda \equiv (1/E_{ign})(\Delta Q/\Delta E)$ is only realized as a hazard when the heat of combustion of the product per unit surface area, H_c (J/m^2), is sufficient to grow the fire. The dimensionless fire hazard of a combustible product of thickness b is therefore, $\Pi = \lambda H_c$, while the fire hazard of the component materials is an average over the product thickness, $\pi = \Pi/b$.

William J. Hughes Technical Center, Aviation Research Division, Federal Aviation Administration, Atlantic City International Airport, NJ, USA

Corresponding author:
Richard E Lyon, William J. Hughes Technical Center, Aviation Research Division, Federal Aviation Administration, Atlantic City International Airport, NJ 08405, USA.
Email: richard.e.lyon@faa.gov richlyon@comcast.net

The measurement of λ, Π, and π from combustion energy diagrams of heat release Q (J/m^2) versus incident energy E (J/m^2) is described, as well as a physical basis for a fire growth potential that provides simple analytic forms for λ in terms of the parameters reported in cone calorimeter tests. Experimental data from the literature show that rapid fire growth in full-scale fire tests of combustible materials occurs above a value of Π determined by the severity of the fire test.

Keywords

Fire growth, cone calorimeter, ignition, burning, large-scale fires, small-scale flammability

Introduction

When considering new materials for occupied spaces, fire performance is one of several factors that must be considered. There are various approaches to assess the passive fire protection capability of materials and their structural elements. The prescribed method is to conduct experiments in accord with the fire standards and regulations.[1–13] Numerical simulations, for example, computational fluid dynamics (CFD)[14] and finite element models coupled to pyrolysis models[15] are another approach that allows researchers to carry out simulations using physical and chemical properties of materials that must be estimated or determined experimentally.[16] More recently, fire performance of combustible materials is being simulated using artificial intelligence, machine learning (ML), and artificial neural networks (ANN),[17] but the descriptors used to train the model may be non-physical or nonsensical.

  The most common method to estimate the fire growth potential of materials is to measure the heat release rate history in fire calorimeters under controlled conditions.[1–5] The cost advantage of using small/bench-scale 0.01-m^2 specimens to predict the outcome of large/full-scale fire tests requiring many square meters of material[6–13] is significant, so various bench-scale fire test parameters have been proposed to rank or classify the flammability and ignitability of combustible materials.[18–32]

  Babrauskas[29] proposed that the flame-spread velocity v_f was proportional to the ratio of the 60-s average areal heat release rate $\dot{Q}_{60s}$ (W/m^2) to the piloted ignition time t_{ign} (s) in a cone calorimeter according to ISO 5660[2] or ASTM E1354[5] at an external heat flux, $\dot{q}_{ext} = 25$ kW/m^2. This flame-spread parameter correlated the two-dimensional (areal) fire growth rate (FIGRA: m^2/s) in full-scale fire tests with limited success, because $\dot{q}_{ext} = 25$ kW/m^2 was below the critical heat flux for ignition $\dot{q}_{crit}$ of some products.

  Cleary and Quintiere[30] measured the test average heat release rate in the cone calorimeter, $\dot{Q}_{avg}$, relative to the critical bench-scale value for upward flame spread, $\dot{Q}_{crit} = 100$ kW/m^2 at an external heat flux, $\dot{q}_{ext} = 50$ kW/m^2, safely above the critical heat flux for ignition $\dot{q}_{ign}$ of most of the combustible materials tested. Quintiere et al. derived a fire growth parameter, $\lambda = 1 + \left(\dot{Q}_{avg}/\dot{Q}_{crit}\right)$, and found that materials exposed to a 100-kW propane burner during the first 10 minutes of a full-scale ISO 9705 room fire test could generate a 1 MW fire (flashover) if $\lambda > 1$, while materials exposed to a 300-kW burner during the next 10 minutes of the full-scale test would reach flashover if, $\lambda \geq t_{ign}/t_b$, where t_b was the total burning time of the sample in the cone calorimeter.[5,31] In Quintiere's theory of fire growth,[30,31] $\dot{Q}_{avg} = HRP\dot{q}_{ext}$, where $HRP = \Delta\dot{Q}_{max}/\Delta\dot{q}_{ext} = \Delta Q/\Delta q_{ext}$, is the slope of maximum/peak heat release rate, $\dot{Q}_{max}$ versus $\dot{q}_{ext}$ obtained from multiple tests. Consequently, Quintiere's fire growth parameter that is used in ASTM E1354[5] to predict large-scale fire performance can

also be written for early stage fire growth as the dimensionless product of a material's combustibility and ignitability as measured in a cone calorimeter, λ = (combustibility) ignitability = $(\Delta Q/\Delta q_{ext})(\dot{q}_{ext}/\dot{Q}_{crit})$.

A Fire Propagation Index (FPI) = $(\dot{Q}_{max}/t_{ign})$[19] and its inverse $(\dot{Q}_{max}/t_{ign})^{-1}$;[27,28] computed from cone calorimeter measurements have been proposed as predictors of the time to reach untenable conditions (flashover) in full-scale room fire tests of furnishings and wall lining materials, where $\dot{Q}_{max}(W/m^2)$ is the maximum/peak heat release rate per unit area measured in a cone calorimeter. More recently, Vahabi et al.[25,26] added the heat of combustion per unit area H_c to the FPI as suggested earlier by Petrella,[20] and obtained a fire retardancy parameter, FR = $\dot{Q}_{max}H_c/t_{ign}$ that improved the correlation of FPI with fire test data.

Tewarson et al.[19] used an FPI = $750\,\dot{Q}^{1/3}/\dot{q}_{net}t_{ign}^2$ measured in a bench-scale fire propagation apparatus ASTM E20584 at net heat flux $\dot{q}_{net}$ to correlate upward fire growth in a full-scale (2.4 m × 0.6 m × 2) parallel panel test that is used to qualify clean room materials for fire safety.9

Numajiri and Furukawa[18] used an empirical function to fit the heat release rate history in a cone calorimeter and used the fitted parameters to compute a Burning Index at a single external heat flux.

Ostman et al.[21,22] used an empirical equation to correlate cone calorimeter data for wood, construction, and wall lining materials measured at an external energy/heat flux $\dot{q}_{ext}$ = 50 kW/m^2 with the time to reach 1 MW heat release rate (flashover) in a full-scale room fire test[6–8] that is used to classify the fire safety of these products.

Shields et al.[24] recognized the importance of ignitability on fire growth and used a flux-time product (FTP) = $t_{ign}\left(\dot{q}_{ext} - \dot{q}_{ign}\right)^N$, to evaluate the critical heat flux for piloted ignition of wood, $\dot{q}_{ign}$, by measuring t_{ign} as a function of $\dot{q}_{ext}$ with N an empirical parameter related to sample thickness. The FTP was shown to be independent of sample orientation with respect to gravity and the mode of ignition (spark or flame).

To bridge the length scale between a bench-scale fire calorimeter (0.01 m^2) and a full-scale room fire test (32 m^2), a quarter-scale fire test using an 8-m^2 sample was developed called the single burning item (SBI).[13] The FIGRA of a material in the SBI test ignited by a gas burner in the corner of a standard fixture was defined as the maximum value of the heat release rate of the SBI divided by the time to reach the maximum heat release rate. The FIGRA value is used to classify the fire safety of building products as A1, A2, B, C, and D in Europe, despite many caveats to the measurement. However, the SBI test, like the room fire test is expensive, so a computer model was developed to calculate the heat release rate of a material or product in the SBI and ISO 9705 test from a single cone calorimeter heat release rate history.[32]

The purpose of bench-, product-, quarter- and full-scale fire tests of combustible solids, as well as numerical modeling of fire growth, is to measure or predict the level of passive fire protection afforded by a specific composition of matter in a particular fire environment. This article attempts to achieve that goal by defining the fire growth potential of a combustible solid as the product of its ignitability and combustibility, and describes a methodology for evaluating the fire growth potential and fire hazard of materials and products using a cone calorimeter under standard[2,5] conditions.

Technical approach

The fire growth of combustible solids is a continuous and coupled process of anaerobic in-depth fuel generation and surface flame spread at a solid–air interface, where the gaseous fuel mixes with oxygen and reacts in a flame to generate heat and products of complete and incomplete combustion. The fuel generation (burning) rate is coupled to the flame-spread rate by heat transfer from the flame or fire to the solid surface, which depends on the angle of inclination with respect to gravity. Figure 1 is an idealized heat release rate ($\dot{Q}$) history for one-dimensional ignition and burning of a sample that is perpendicular to gravity under steady (1(a)) and unsteady (1(b)) conditions at a constant incident energy flux $\dot{q}_{ext}$ imposed at time $t = 0$. The time-integrated histories of $\dot{Q}$ and the radiant energy flux, $\dot{E}_0 = \dot{q}_{ext}$ of Figure 1(a) and (b) are plotted as energy diagrams of Q versus the nominal incident thermal energy, $E_0 = \dot{q}_{ext}t$, for the steady and unsteady processes in Figure 1(c) and (d). The nominal energy absorbed by the sample at the time of ignition, t_{ign}, is $E_{ign,0} = \dot{q}_{ext} \, t_{ign}$ and $E_{f,0} = \dot{q}_{ext} \, t_f$, is the incident energy at the end of burning t_f when the flame extinguishes. Steady burning as in Figure 1(a) is analogous to a phase change at constant temperature, for which the boundary conditions at the surface $x = 0$ and the rear face $x = b$ remain constant. Steady burning is rarely (if ever) observed for solids in the cone calorimeter because of the transient temperature gradient due to finite sample thickness and thermal insulation at $x = b$, and re-radiation of incident energy at the fire-exposed surface $x = 0$. The slope of the energy diagrams of Figure 1(c) and (d) is $\Delta Q/\Delta E_0$ which is the amount of combustion heat generated per unit input of thermal energy, that is, the combustibility.

If the ignitability of a combustible solid in the cone calorimeter is $1/E_{\mathrm{ign},0}$ (m^2/MJ) and its combustibility is $\Delta Q/\Delta E_0$ (dimensionless), then its potential for sustained ignition and burning, that is, fire growth, is the product of the following terms

$$\text{Fire growth potential, } \lambda \equiv (1/E_{ign,0})(\Delta Q/\Delta E_0) \tag{1}$$

Equation (1) is the integral analog of Quintiere's[30,31] dynamic fire growth parameter, which showed good capability to predict flashover of materials in room fire tests using cone calorimeter data. In the present context, the potential for fire growth is only realized as a fire hazard if the total heat of combustion per unit area burning surface, H_c (MJ/m^2), is sufficient to sustain the fire, so the dimensionless fire hazard of a material or product is

$$\text{Product fire hazard} = \Pi \equiv \lambda H_c \tag{2}$$

The material fire hazard is an average over the sample thickness, b, obtained from the volumetric heat of combustion, $H_{c,V}$ (MJ/m^3)

$$\text{Material fire hazard} = \pi = \lambda H_{c,V} = \Pi/b \tag{3}$$

The potential of a material or product to grow a fire to hazardous conditions is calculable from cone calorimeter heat release rate histories using equations (1)–(3), with $\Delta Q/\Delta E$ the maximum slope of an energy diagram constructed from a plot of the time integral of the heat release rate history, $Q(t) = \int \dot{Q}(x)dx$ versus the time integral of the thermal energy deposition rate at constant energy flux, $E(t) = \int \dot{q}_{ext}dx = \dot{q}_{ext}t$, measured in the cone calorimeter, and $E_{ign} = E(t_{ign})$ the ignition energy at the onset of the integral curve (see Figure 1).
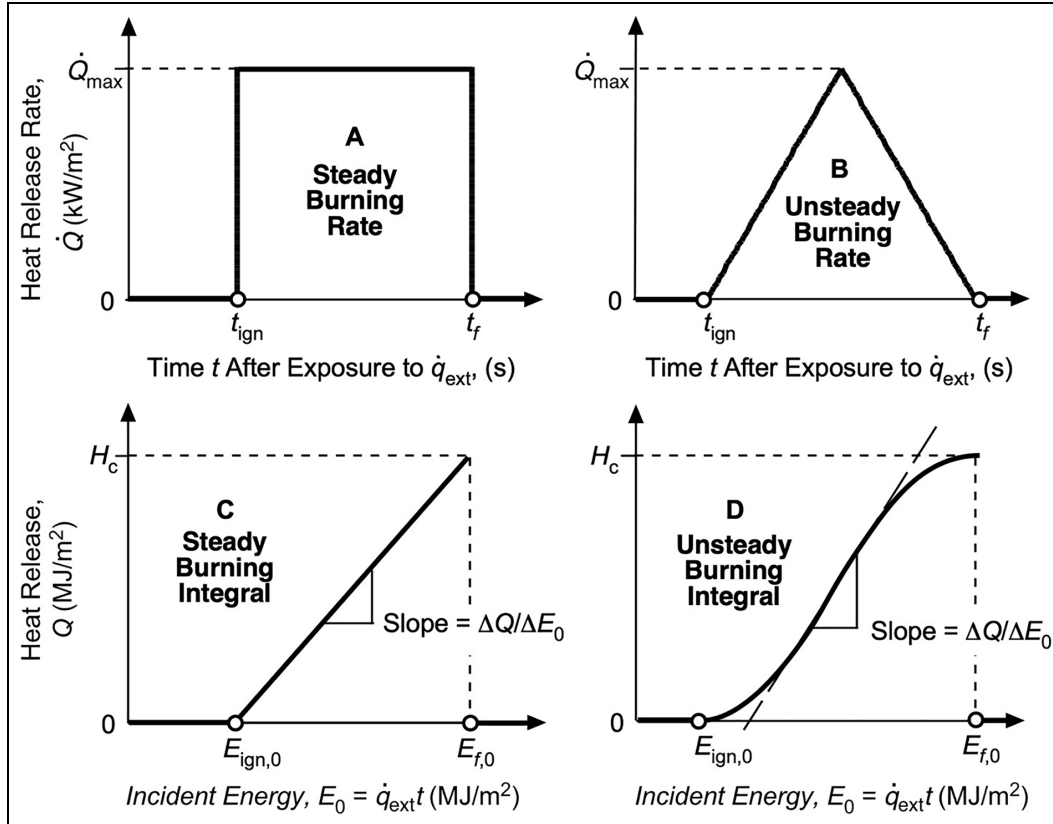
Figure 1. Idealized heat release histories for steady (A,C) and unsteady (B,D) burning.

Experimental

Methods

Tests were conducted in our laboratory at the Federal Aviation Administration (FAA) Technical Center in triplicate on 10 cm × 10 cm square samples of various (typically 3.2 mm) thickness in a cone calorimeter from Fire Testing Technology, East Grinstead, UK, according to the standard method.[5] A sample holder with edge frame and wire grid, insulated rear sample face, and an electric spark igniter were used for all tests. Cone calorimeter results from the literature were reportedly obtained under similar conditions. Gases used for calibration and testing were high purity grades from local suppliers. The nomenclature and units of cone calorimeter quantities used in this article, in ASTM E1354, and in the literature are listed in Table 1 as symbols and acronyms.

Materials

The unmodified (natural) polymers in Table 2 contain no flame retardant (NFR) additives or fillers and minimal processing aids, and were obtained in sheet form having nominal thickness of 3.2, 6.4, 12.5, or 25 mm, from commercial suppliers. Sixteen polymers were obtained from commercial suppliers or manufacturers. The flame-retardant polystyrene (PS-BFR) and PC/ABS blends were provided by research partners.

Table 1. Description and nomenclature of cone calorimeter measurements.

Quantity	Symbol	Acronym	ASTM E1354	Units
External energy (heat) flux	$\dot{q}_{ext}$	EHF	–	W/m^2
Heat release rate per unit area	$\dot{Q}$	HRR	$\dot{q}''$	W/m^2
Heat released per unit area at time t	$Q(t)$	–	–	J/m^2
Incident energy	$\dot{q}_{ext}t$	$E(t)$	–	J/m^2
Critical energy flux for piloted ignition	$\dot{q}_{ign}$	CHF	–	W/m^2
Critical energy flux for sustained burning	$\dot{q}_{burn}$	–	–	W/m^2
Time to piloted ignition	t_{ign}	TTI	t_{ig}	s
Ignition energy	$\dot{q}_{ext}t_{ign}$	E_{ign}	–	J/m^2
Peak heat release rate	$\dot{Q}_{max}$	PHRR	$\dot{q}''_{max}$	W/m^2
Test average heat release rate	$\dot{Q}_{avg}$	HRR$_{avg}$	–	W/m^2
Total heat release/fire load	H_c	THR	q''_{total}	J/m^2

ASTM: American Society for Testing and Materials.

Table 2. Polymers tested at FAA for this study.

Polymer	Symbol	Polymer	Symbol
Acrylonitrile-butadiene-styrene polymer	ABS	Poly(hexamethylene adipamide)	PA66
High-density polyethylene	HDPE	Poly(vinylidenefluoride)	PVDF
Polypropylene	PP	Poly(oxymethylene)	POM
PS with 20% Decabromodiphenyloxide	PS-BFR	Poly(phenylsulfone)	PPSU
High impact polystyrene	HIPS	Poly(phenylenesulfide)	PPS
Poly(methylmethacrylate)	PMMA	Poly(vinylchloride)	PVC
Polycarbonate of bisphenol-A	PC	Polyetherimide	PEI
PC/ABS blends	PC/ABS	Polyetheretherketone	PEEK
Poly(ethylene terephthalate)	PET	Fluorinated ethylene propylene	FEP

ABS: acrylonitrile-butadiene-styrene polymer; HDPE: high-density polyethylene; PVDF: poly(vinylidenefluoride); PP: polypropylene; POM: poly(oxymethylene); PPSU: poly(phenylsulfone); HIPS: high impact polystyrene; PPS: poly(phenylenesulfide); PMMA: poly(methylmethacrylate); PVC: poly(vinylchloride); PC: polycarbonate; PEI: polyetherimide; PEEK: polyetheretherketone; PET: poly(ethylene terephthalate); FEP: fluorinated ethylene propylene.

Results

Figure 2 is a composite of $\dot{Q}$ histories at four different energy/heat flux levels $\dot{q}_{ext}$ for the non-charring polymer poly(methylmethacrylate) (PMMA) containing black pigment in a cone calorimeter according to the standard methods.[2,5] Figure 3 is a composite energy diagram of the PMMA data in Figure 2 plotted as per Figure 1(d), whose ordinate Q is the time integrated heat release rate history $\dot{Q}$ and whose abscissa E_0 is the nominal value of the time integrated thermal energy flux, $\dot{E}_0 = \dot{q}_{ext}$ indicated in the legend of Figure 2.

Figure 4 is a composite of heat release rate histories for 3-mm thick samples of the charring polymer, polycarbonate of bisphenol-A at the indicated external energy flux, $\dot{q}_{ext}$ = EHF. Figure 5 is the energy diagram for the data in Figure 4 obtained by time integration of the ordinate $\dot{Q}$ and the abscissa $\dot{E}$ = $\dot{q}_{ext}$.

Energy diagrams like Figures 3 and 5 were constructed and evaluated for the 16 charring and non-charring polymers in Table 2 to obtain the nominal ignition energy, $E_{ign,0}$ = $\dot{q}_{ext}\,t_{ign}$
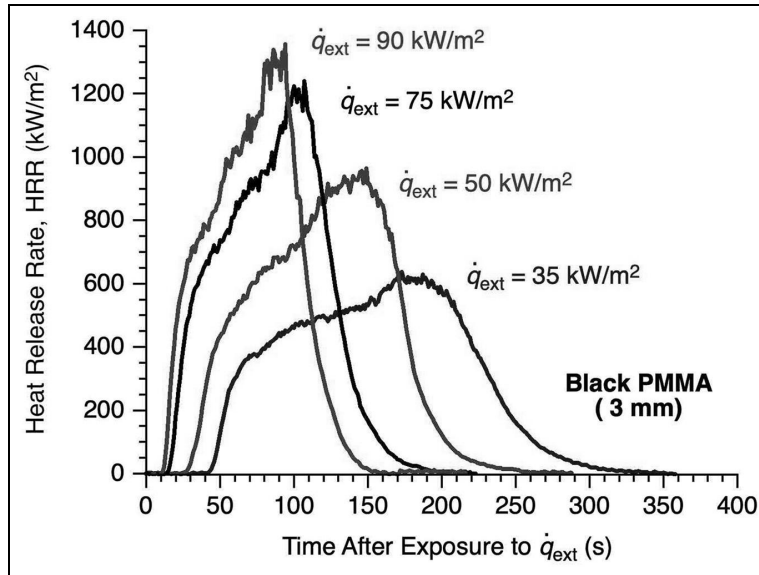
Figure 2. Heat release rate histories of black PMMA in cone calorimeter at $\dot{q}_{ext}$ = 35, 50, 75, and 90 kW/m². Each plot is an average of three experiments.
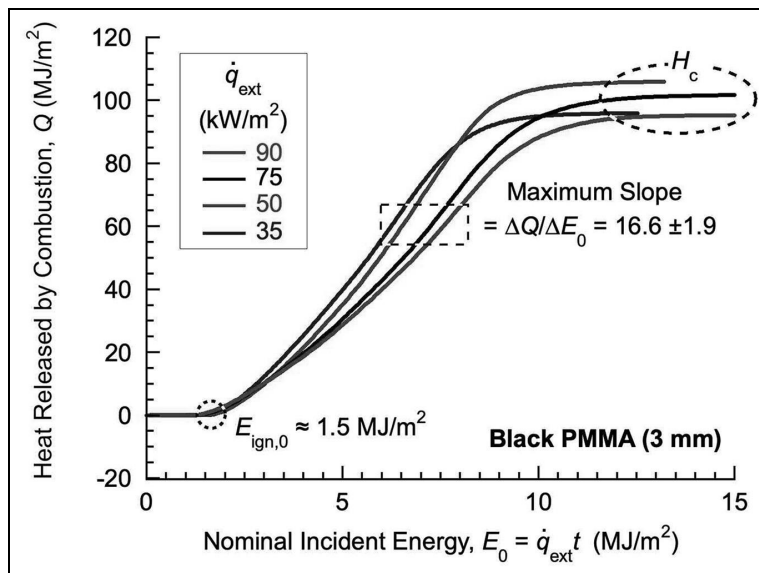

Figure 3. Cone calorimeter energy diagram of heat release versus incident energy for the non-charring polymer PMMA showing nominal ignition energy ($E_{ign,0}$), combustibility ($\Delta Q/\Delta E_0$), and heat of combustion (H_c).

and combustibility, $\Delta Q/\Delta E_0$, as per Figure 1(d) for computing λ by equation (1). The λ results from the cone calorimeter energy diagrams at $\dot{q}_{ext}$ = 50 kW/m² are plotted in Figure 6, which show a three order of magnitude range for the polymers in Table 2.
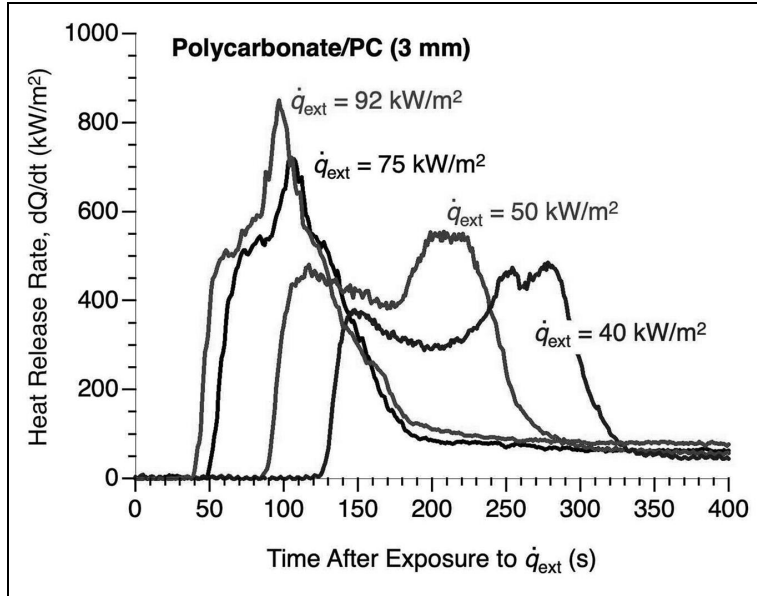
Figure 4. Heat release rate histories of the char forming polymer PC in cone calorimeter at $\dot{q}_{ext}$ = 40, 50, 75, and 92 kW/m². Each plot is an average of three experiments.
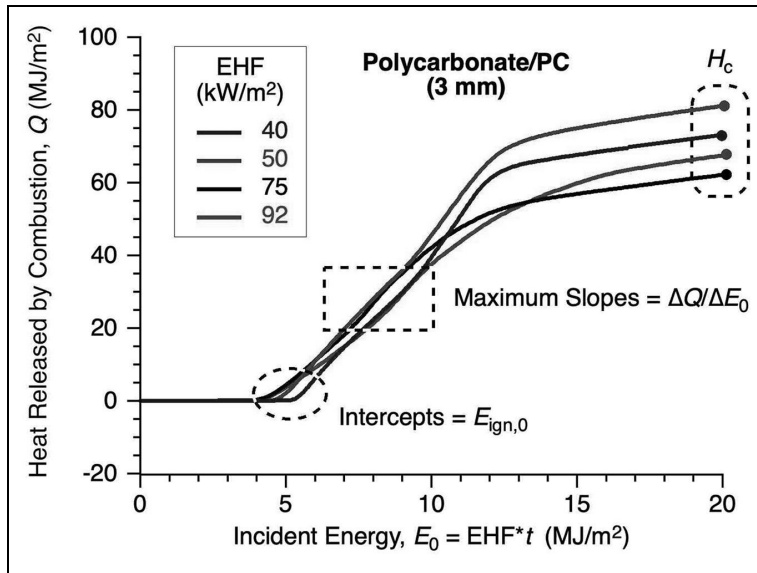

Figure 5. Cone calorimeter energy diagram of heat release versus incident energy for the char forming polymer PC showing nominal ignition energy ($E_{ign,0}$), combustibility ($\Delta Q/\Delta E_0$), and total heat of combustion (H_c).

A physical basis for fire growth potential

Figure 6 shows that energy diagrams such as Figures 3 and 5 provide repeatable estimates of λ for unsteady burning that can be used to compare and rank the fire growth potential of materials, but numerical integration of heat release rate histories, $\dot{Q}(t)$ at one or more radiant energy fluxes, $\dot{q}_{ext}$ versus time is required. This metrology, while trivial with modern
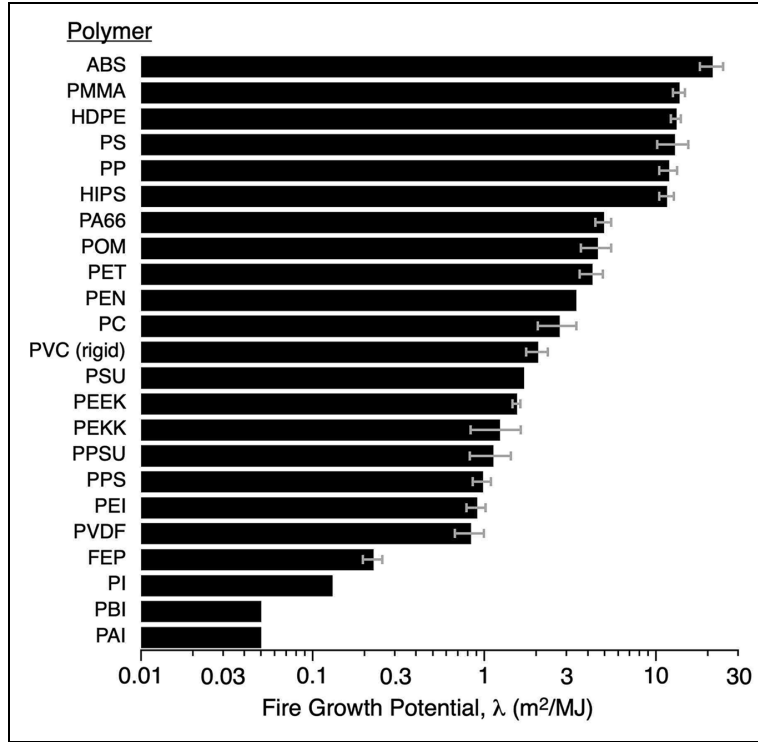
Figure 6. Fire growth potential computed from energy diagrams at external energy flux, $\dot{q}_{ext}$ = 50 kW/m^2. Error bars are $\pm$ one standard deviation for triplicate measurements.

computational resources, does not leverage the large amount of cone calorimeter data that has been reported in the literature parametrically as the maximum/peak heat release rate in the test, $\dot{Q}_{max}$, the time to piloted ignition, t_{ign}, and the total heat released by burning, H_c, at one or more radiant energy fluxes, $\dot{q}_{ext}$, or sample thicknesses, b (see Figure 1 and Table 1) for a wide variety of materials. For this reason, a physical basis for fire growth potential is derived from the formalisms of thermal ignition and steady burning of liquids and solids that provides analytic forms for λ, Π, and π in terms of cone calorimeter parameters in the published literature or obtained directly from standard[2,5] test reports.

Begin with the assumption that the steady-state heat release rate per unit area $\dot{Q}_{ss}$(W/m^2) of Figure 1(a) is related to the steady mass loss (burning) rate per unit area $\dot{m}_{ss}$ (kg/m^2-s) and the specific heat of combustion of the fuel gases with oxygen in a diffusion flame h_c (J/kg)[33,34]

$$\dot{Q}_{ss} = \dot{m}_{ss} h_c \tag{4}$$

By convention, the fluxes of combustion heat ($\dot{Q}$) and volatile fuel mass ($\dot{m}_{ss}$) are positive, as is the specific heat release by flaming combustion (h_c). After the fuel gases at the solid surface ignite, a diffusion flame attaches to the surface and the mass flux is proportional to the net surface heat flux ($\dot{q}_{net}$) and inversely proportional to the energy required to thermally decompose the solid to gaseous fuel and vaporize the products, h_g (J/kg), at the burning temperature, T_{burn}. For steady burning[33,34]

$$\dot{m}_{ss} = \frac{\dot{q}_{net}}{h_g} \tag{5}$$

Substituting equation (5) into equation (4) for a solid of surface area S, density ρ, and thickness b, the steady heat release rate is

$$\dot{Q}_{ss} = \frac{h_c}{h_g}\dot{q}_{net} = \left(\frac{\chi}{\alpha}\right)\left(\frac{\rho b h_c}{\rho b h_g}\right)\dot{q}_{net} = \left(\frac{H_c}{L_g}\right)\dot{q}_{net} \qquad (6)$$

In equation (6), $\chi/\alpha \approx 1$ is the ratio of the combustion efficiency in a diffusion flame under well-ventilated (cone calorimeter) conditions, χ, to the efficiency of radiant and convective energy transfer to the solid at the nominal irradiance in a cone calorimeter, $\alpha = \dot{q}_{net}/\dot{q}_{ext}$. The slope of a plot of $\dot{Q}_{ss}$ *versus* $\dot{q}_{net}$ is called the combustibility ratio[35] or the heat release parameter.[23] It is the ratio of the heat released by combustion of the fuel gases in air to the energy consumed to generate the fuel gases in the solid during burning on a mass (h_c/h_g) or surface area (H_c/L_g) basis. Once ignition has occurred and burning has commenced, the surface temperature of the solid at $x = 0$ increases from the ignition temperature T_{ign} to the burning temperature T_{burn}, due to the presence of the flame, while the solid at the back of the pyrolysis zone, $x = \delta$, remains at the ignition temperature, T_{ign}. Both T_{burn} and T_{ign} are determined by the chemical kinetics of thermal decomposition of the solid.[37–39]

Equation (6) is predicated on the existence of a steady heat release rate $\dot{Q}_{ss}$, which is rarely if ever observed for finite thickness solids in practice. Alternatively, steady heat release rate in a cone calorimeter can be approximated as a time average of the heat release rate history $\dot{Q}(t)$ over the test duration, $\dot{Q}_{avg}$,[30,31,40] or a moment average in the vicinity of the maximum/peak heat release rate $\dot{Q}_{max}$[41]

$$\dot{Q}_{ss} = \frac{5}{2\sqrt{3}}\dot{Q}_{avg} = \frac{1}{\sqrt{3}}\dot{Q}_{max} \qquad (7)$$

The thermal theory of ignition assumes the ignition temperature T_{ign} is a property of the material, consistent with the kinetic basis for T_{ign} as the temperature at the onset of thermal decomposition of the solid.[37,38,41,42] Consequently, the time required for the surface of a solid of thickness b, specific heat c_P, and thermal conductivity κ, initially at temperature T_0 to reach T_{ign} when exposed to a constant net heat flux $\dot{q}_{net}$ at $t = 0$ in a cone calorimeter increases with the thermal stability of the solid and is obtained from unsteady heat conduction as the time to ignition, t_{ign}[33,34]

$$t_{ign} = \begin{bmatrix} \rho c_P b T_{ign}/\dot{q}_{net} & (thermally\,thin, b<\delta) \\ \rho c_P \kappa \left(T_{ign}/\dot{q}_{net}\right)^2 & (thermally\,thick, b \geqslant \delta) \end{bmatrix} \qquad (8)$$

In equation (8), δ is the depth of the pyrolysis layer for steady burning[37,38]

$$\delta = \frac{\kappa \Delta T_{burn}}{\dot{q}_{net}} \qquad (9)$$

The energy barrier to ignition (ignition energy) in a cone calorimeter is the amount of thermal energy that has entered the surface of the combustible solid at the time of ignition t_{ign}. For a constant external energy flux in the cone calorimeter $\dot{q}_{ext}$ applied at time $t = 0$ that is above the critical energy flux for ignition, $\dot{q}_{ign}$, the net energy flux is $\dot{q}_{net} = \dot{q}_{ext} - \dot{q}_{ign}$ and the ignition energy is

$$E_{ign} \equiv \int_0^{t_{ign}} \dot{E}dt = \int_0^{t_{ign}} \dot{q}_{net}dt = \dot{q}_{net}t_{ign} \tag{10}$$

Equations (4)–(10) describe the ignitability ($1/E_{ign}$) and combustibility ($\dot{Q}_{ss}/\dot{q}_{net}$) in terms of the energy supplied to, and the combustion heat released from, a steadily burning solid in a fire or fire calorimeter. If the heat of combustion of the volatile fuel and the energy to thermally decompose and gasify the solid fuel, E_{dec}, do not change during steady burning at T_{burn}, then, $\Delta Q \approx H_c$, and $\Delta E = E - E_{ign} = (E_{ign} + E_{dec}) - E_{ign} = L_g$.[36] Ignition and in-depth burning are the coupled processes that drive flame spread, so it is the product of ignitability and combustibility that is the definition of the potential for fire growth of equation (1)

$$\text{Fire growth potential, } \lambda \equiv \left(\frac{\Delta Q}{\Delta E}\right)\left(\frac{1}{E_{ign}}\right) \approx \left(\frac{H_c}{L_g}\right)\left(\frac{1}{E_{ign}}\right) = \left(\frac{\dot{Q}_{ss}}{\dot{q}_{net}}\right)\left(\frac{1}{\dot{q}_{net}t_{ign}}\right) \tag{11}$$

The product of the denominators in the last term of equation (11) is the FTP at ignition, FTP $= t_{ign}\dot{q}_{net}^N$, for a thermally thick ($N = 2$) sample at a constant net heat flux.[24] The FTP is independent of sample orientation with respect to gravity (vertical or horizontal) and the mode of ignition (spark or flame). Substituting equation (8) for the time to ignition for $b \geqslant \delta$ into equation (10) gives the ignition energy for a thermally thick combustible solid

$$E_{ign} = \frac{\rho c_P \kappa \Delta T_{ign}^2}{\dot{q}_{net}} = \frac{\rho c_P \kappa \Delta T_{ign}^2}{\dot{q}_{ext} - \dot{q}_{ign}} \tag{12}$$

The numerator of Equation 12 is the square of what is called the thermal response parameter, TRP.[23,31] Substituting equation (12) into equation (11) gives the fire growth potential of a thermally thick combustible solid capable of steady burning

$$\lambda = \frac{H_c/L_g}{E_{ign}} = \left[\frac{h_c/h_g}{\rho c_P \kappa \Delta T_{ign}^2}\right]\dot{q}_{net} = K\dot{q}_{net} = K\left(\dot{q}_{ext} - \dot{q}_{ign}\right) \tag{13}$$

Equation (13) is a constitutive relationship for the fire response λ to the thermal stress of a fire $\dot{q}_{net}$ of a combustible solid having fire compliance K. The fire growth potential λ is independent of sample thickness because the chemical reactions that consume energy to generate volatile fuel are confined to a thin surface layer $\delta << b$ for burning at $\dot{q}_{ext} > 50$ kW/m^2 (typically), and the rate of these anaerobic reactions depends primarily on temperature. The fire response of a thermally thin solid is obtained from equations (8), (10), and (11) as

$$\lambda' = \frac{1}{b}\left[\frac{h_c/h_g}{\rho c_P \Delta T_{ign}}\right] = \frac{K'}{b} \text{ (thermally thin)} \tag{14}$$

The fire response λ' of a thin sample, $b < \delta$ is independent of thermal stress $\dot{q}_{net}$ and inversely proportional to the sample thickness b. The fire compliance K of equation (13) and K' of equation (14) are intensive properties because they are independent of the amount of combustible material, the sample orientation with respect to gravity, and the mode of ignition.

Unlike the fire growth potential λ and material fire hazard, the product fire hazards Π is not an intensive property because it depends on the mass or thickness of the sample, that is, the fire load, H_c (see equations (2) and (3)).

Analytic forms for λ

At ignition the net flux of thermal energy $\dot{q}_{net}$ entering a surface exposed to a constant radiant/convective energy flux from an external heater or fire will be a fraction α of the incident energy, $\dot{q}_{ext}$, due to losses from the surface by re-radiation and convection, $\dot{q}_{ign}$

$$\dot{q}_{net}(ignition) = -\kappa\left(\frac{dT}{dx}\right) = \kappa\frac{\Delta T_{ign}}{\delta} = \dot{q}_{ext} - \dot{q}_{ign} \equiv \alpha\dot{q}_{ext} \tag{15}$$

In equation (15), α is the coupling efficiency of the incident energy with the combustible solid. According to equations (10) and (15), the thermal energy absorbed by a solid in a cone calorimeter experiment at the time of ignition t_{ign} is related to the nominal value of the ignition energy, $E_{ign,0}$, at constant $\dot{q}_{ext}$

$$E_{ign} = \alpha E_{ign,0} = \alpha\dot{q}_{ext}t_{ign} \tag{16}$$

At the onset of burning the flame adds an additional energy flux that increases the surface temperature from T_{ign} to T_{burn}.[37] The corresponding change in the surface temperature with respect to ambient T_0 is, $\Delta T_{ss} = (T_{burn} - T_0) = (T_{burn} - T_{ign}) + (T_{ign} - T_0) = \Delta T_{burn} + \Delta T_{ign}$. If the heat flux from the flame provides all the energy required to thermally decompose the solid in the pyrolysis layer and gasify the products, $\kappa\Delta T_{burn}/\delta = \dot{m}h_g$[37]

$$\dot{q}_{net}(burning) = \left\{\kappa\frac{\Delta T_{burn}}{\delta} - \dot{m}h_g\right\} + \kappa\frac{\Delta T_{ign}}{\delta} \approx \kappa\frac{\Delta T_{ign}}{\delta} = \alpha\dot{q}_{ext} \tag{17}$$

Substituting equations (7), (16), and (17) into equation (11)

$$\lambda \equiv \frac{H_c/L_g}{E_{ign}} = \frac{1}{\alpha}\left(\frac{\Delta Q/\Delta E_0}{E_{ign,0}}\right) = \frac{1}{\alpha^2}\left(\frac{5}{2\sqrt{3}}\frac{\dot{Q}_{avg}}{\dot{q}_{ext}^2 t_{ign}}\right) = \frac{1}{\alpha^2}\left(\frac{1}{\sqrt{3}}\frac{\dot{Q}_{max}}{\dot{q}_{ext}^2 t_{ign}}\right) \tag{18}$$

Equation (18) allows calculation of steady state λ at constant $\dot{q}_{ext}$ from the slope of combustion heat versus the incident thermal energy, $\Delta Q/\Delta E_0$, or the test average heat release rate, $\dot{Q}_{avg}$, or the maximum/peak heat release rate in the test, $\dot{Q}_{max}$.

The coupling efficiency for a material in a cone calorimeter experiment α is probably in the range, $\frac{1}{2} < \alpha < 1$ for charring and non-charring materials, respectively.[40,43,44] Therefore, to a first approximation, $\alpha = \frac{3}{4}$ and $\sqrt{3}\alpha^2 \approx 1$ in equation (18), so the material fire response (λ) and product fire hazard (Π) can be expressed solely in terms of quantities that are measured in a standard cone calorimeter test

$$\lambda_{NRG} \equiv \frac{1}{\alpha}\left(\frac{\Delta Q/\Delta E_0}{E_{ign}}\right) \approx \frac{4}{3}\frac{\Delta Q/\Delta E_0}{\dot{q}_{ext}t_{ign}} \tag{19}$$

$$\lambda_{AVG} \equiv \frac{1}{\alpha^2 \sqrt{3}} \left(\frac{5}{2} \frac{\dot{Q}_{avg}}{\dot{q}_{ext}^2 t_{ign}} \right) \approx \frac{5}{2} \frac{\dot{Q}_{avg}/t_{ign}}{\dot{q}_{ext}^2} \qquad (20)$$

$$\lambda_{MAX} \equiv \frac{1}{\alpha^2 \sqrt{3}} \left(\frac{\dot{Q}_{max}}{\dot{q}_{ext}^2 t_{ign}} \right) \approx \frac{\dot{Q}_{max}/t_{ign}}{\dot{q}_{ext}^2} \qquad (21)$$

According to equation (2), the product fire hazards Π_j for j = energy (NRG) diagram, AVG and MAX of equations (19)–(21) are

$$\Pi_j = \lambda_j H_c \qquad (22)$$

The fire growth potential (λ) as well as the product fire hazard (Π, π) of equations (19)–(22) were evaluated using cone calorimeter heat release rate histories obtained in our laboratory for the 16 charring and non-charring polymers in Table 2, as well as cone calorimeter data from the published literature.

Figure 7 compares equations (19)–(21) for computing λ from cone calorimeter measurements for 16 of the polymers in Table 2 that are not blends or flame retardant. These polymers were tested in the cone calorimeter according to the standard method[2,5] in triplicate at 3.2-mm thickness and at the typical heat flux reported in the literature, $\dot{q}_{ext}$ = 50 kW/m^2. The λ_j are ranked in descending order from top to bottom by λ_{MAX} (equation (21)). The three forms of λ in Figure 7 obtained from the steady heat release rate and coupling efficiency approximations (equations (19)–(21)) are in qualitative agreement with each other and the integral values for each polymer in Figure 6.

Note that the coupling efficiency approximation of the fire growth potential obtained from the energy (NRG) diagram, λ_{NRG}, equation (19), differs from the definition of λ (equation (1)) by a factor of 4/3. This bias, and the desire to maximize the use of published cone calorimeter data, suggest the steady-state approximation, $\lambda = \lambda_{MAX}$ (equation (21)) be used for computing fire growth potential—a convention that is used in the following plots and analyses unless otherwise specified.

Validation

Non-charring polymers

Figure 8 is a plot of ASTM E1354 cone calorimeter results for cast, black pigmented, polymethylmethacrylate/PMMA at 3, 6, and 25-mm nominal thickness at the external energy flux, $\dot{q}_{ext}$ = 50 kW/m^2. The material response to incident thermal energy from a radiant heater or fire for PMMA, λ, is plotted on the left-hand ordinate of Figure 8. These samples are thermally thick at $\dot{q}_{ext}$ = 50 kW/m^2 because $b > \delta \approx \kappa \Delta T_{burn}/\dot{q}_{ext}$ = 1 mm for DT_{burn} = 200 K[38], κ = 0.2 W/m-K, so λ is independent of thickness in agreement with equation (13). Conversely, the product fire hazard Π on the right-hand ordinate is proportional to sample thickness/fire load as per equations (2) and (22).

Figure 9 is a plot of λ computed from published ASTM E1354 data[43] obtained in our laboratory for clear extruded PMMA at nominal thickness, b = 3, 9, and 27-mm exposed to external energy fluxes, $\dot{q}_{ext}$ = 25, 50, and 75 kW/m^2. These samples are thermally thick under all conditions as per equation (8), as evidenced by the insensitivity of λ to b and the linear relationship between λ and $\dot{q}_{ext}$, as per the constitutive relation for fire growth,
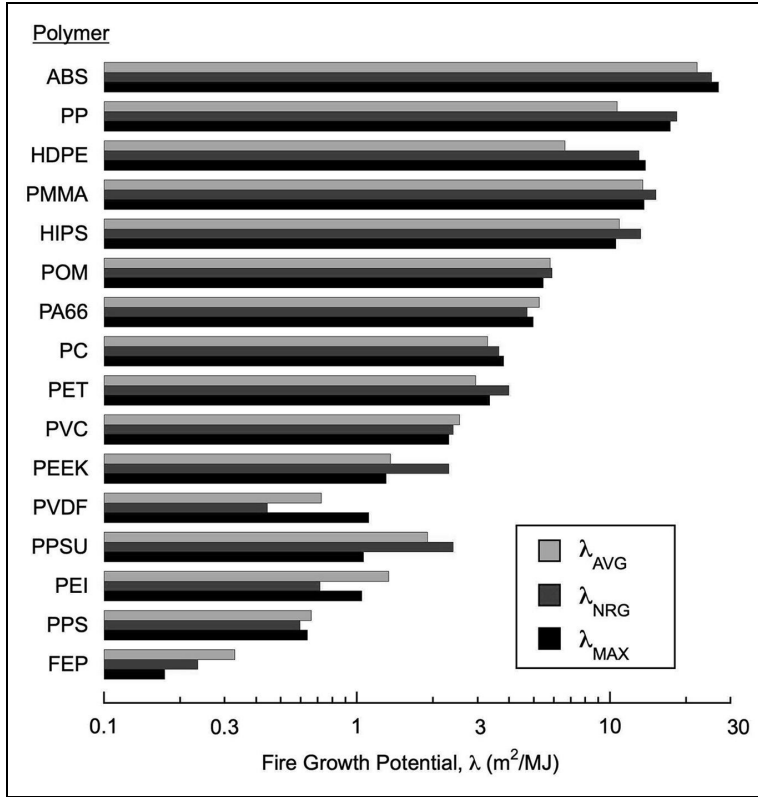
Figure 7. Fire growth potential λ of 16 polymers in Table 2 tested as 3.2-mm samples in triplicate at the typical external energy flux, $\dot{q}_{ext}$ = 50 kW/m^2. Average coefficient of variation of λ_j for each individual polymer is less than 20%.
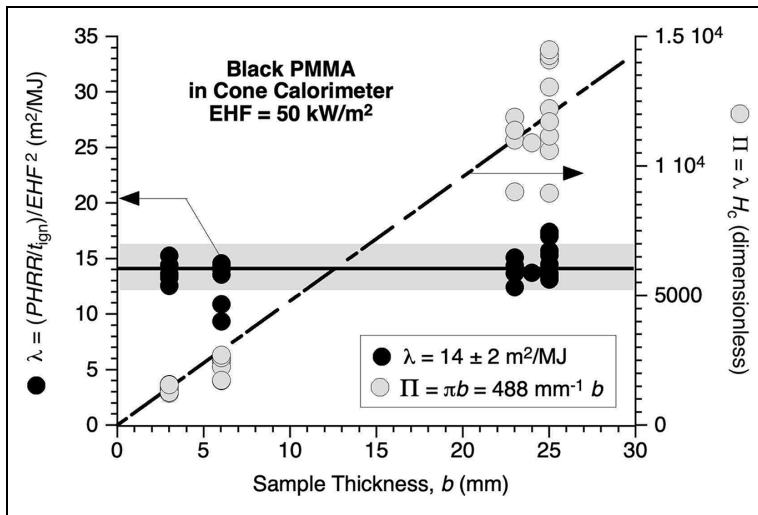

Figure 8. Fire growth potential λ and product fire hazard Π *versus* sample thickness b for black PMMA at EHF = 50 kW/m^2.
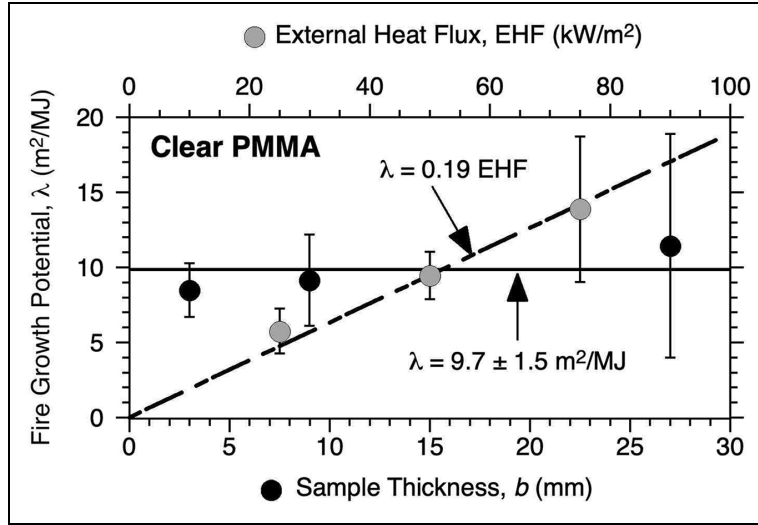
Figure 9. Fire growth potential λ *versus* external heat flux ($\dot{q}_{ext}$ = EHF) and sample thickness (b) for clear PMMA in ASTM E1354. The EHF and b lines intersect at EHF* = 51 kW/m^2.

equation (13). The zero-slope line of λ versus b and the linear fit to $\dot{q}_{ext}$ = EHF intersect at EHF* = 51 kW/m^2. Error bars are one standard deviation of the average value with respect to the independent variable on the opposite abscissa.

Figure 10 is a plot of the nominal ignition energy, $E_{ign,0}$ = $\dot{q}_{ext}t_{ign}$ = EHF t_{ign} for clear PMMA at the same values of b and EHF shown in Figure 8. The horizontal line for λ versus b and a power law fit, $E_{ign,0} \propto$ EHF^{-1} as per equation (12), intersect at EHF* = 41 kWm^2. Error bars are one standard deviation of the indicated average with respect to the independent variable on the opposite abscissa.

Figure 11 is a plot of $E_{ign,0}$ and λ versus sample thickness b = 3, 9, and 27 mm and external heat flux $\dot{q}_{ext}$ = EHF = 25, 50, and 75 kW/m^2 for HIPS and HDPE in ASTM E1354. Cone data are from Stoliarov et al.[43] Graphs for high-impact polystyrene/HIPS are on the left-hand side and graphs for high-density polyethylene/HDPE are on the right-hand side. As indicated by the horizontal line at the global mean for these non-charring polymers, $E_{ign,0}$ and λ are independent of sample thickness b in accordance with equations (12) and (13) for thermally thick burning, because $\delta << b$ and the chemical reactions that produce volatile fuel are confined to a thin surface layer (the pyrolysis zone). The inverse dependence of ignition energy on external heat flux, $E_{ign,0} \propto$ EHF$^{-1.3}$ is consistent with equation (12). Error bars on the data points are one standard deviation of the mean with respect to the independent variable b on the opposite abscissa.

Charring polymers

Combustible materials that leave a solid residue as a pyrolysis product on a burning surface do not generally exhibit steady burning due to the change in the surface boundary condition resulting from the accumulation of solid residue, which is usually of low density and insulates the underlying polymer, as well as re-radiating some of the incident energy from a heater, surface flame; or fire.[16,40] However, the time-dependent burning rate of charring materials is amenable to a moment-area representation of (steady) burning[41] as per equation (7). The fire
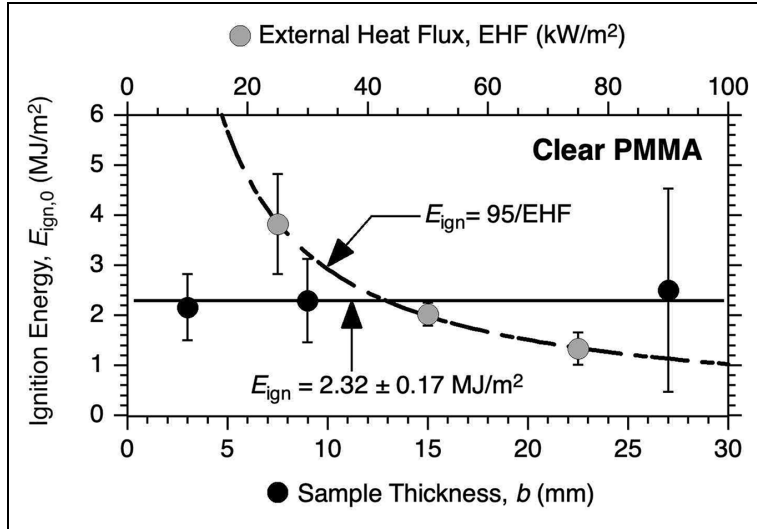
Figure 10. Nominal ignition energy $E_{ign,0}$ versus external heat flux ($\dot{q}_{ext}$ = EHF) and sample thickness (*b*) for clear PMMA. The EHF and *b* lines intersect at EHF* = 41 kW/m^2.
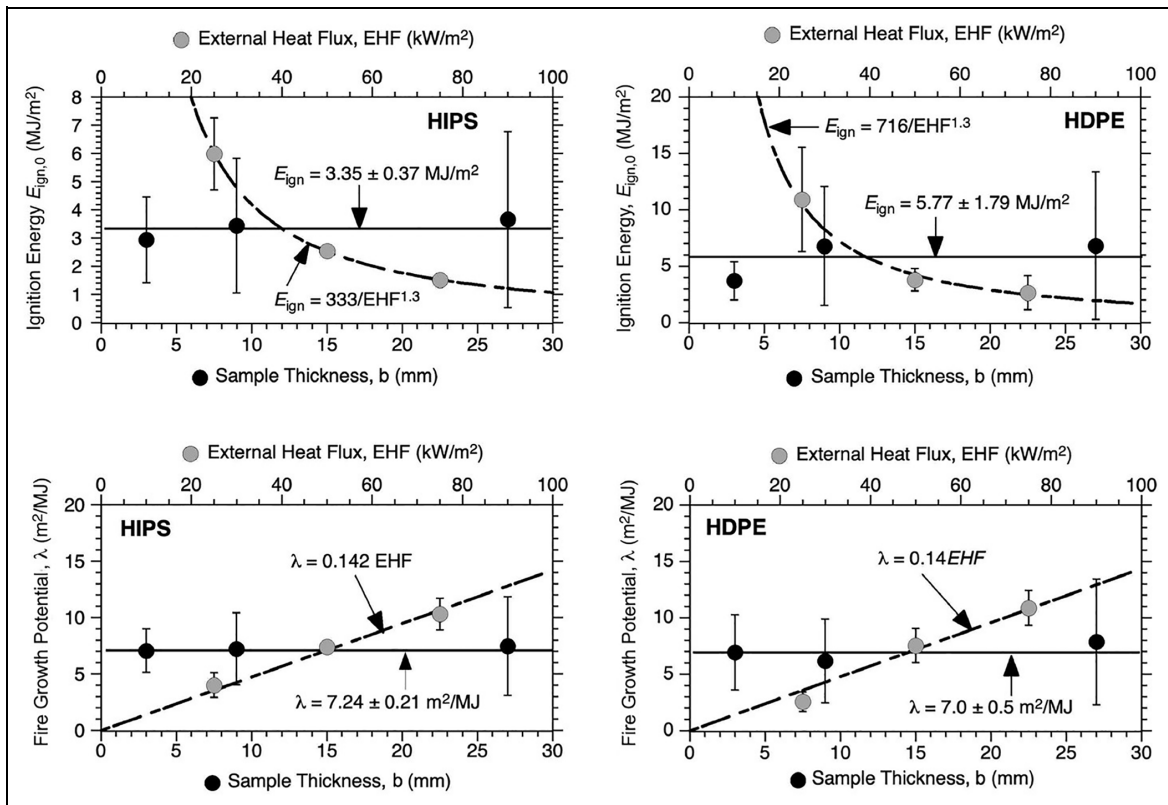

Figure 11. Nominal ignition energy $E_{ign,0}$ and fire growth potential λ of high-impact polystyrene/HIPS and high-density polyethylene/HDPE *versus* external heat flux ($\dot{q}_{ext}$ = EHF) and sample thickness (*b*) in ASTM E1354. Error bars are one standard deviation of the mean value (data point) with respect to the independent variable on the opposite abscissa.
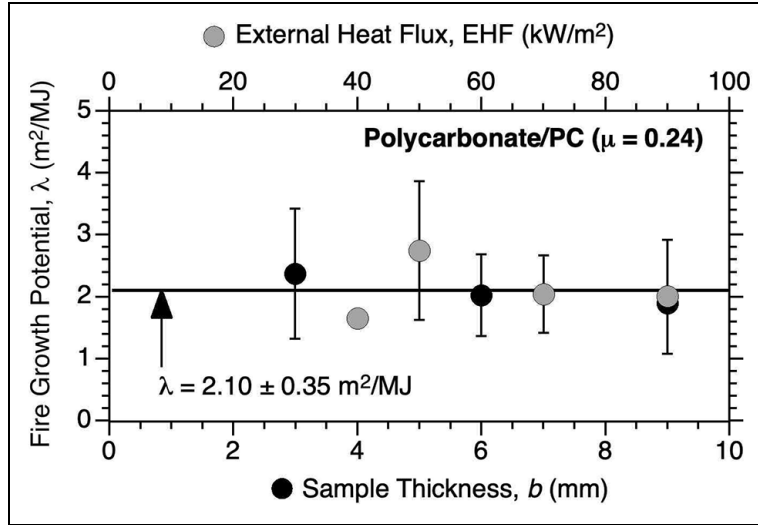
Figure 12. Fire growth potential λ *versus* external heat flux (EHF) and sample thickness (b) for PC in ASTM E 1354 from three different laboratories.[27,44,45]
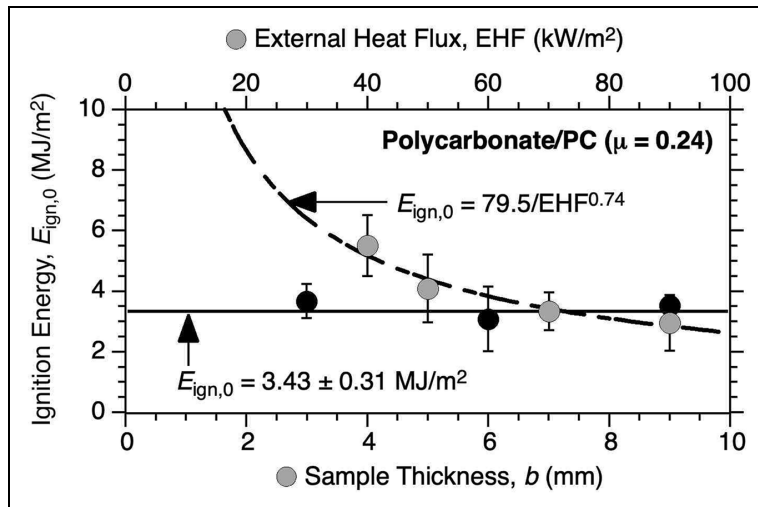

Figure 13. Nominal ignition energy $E_{ign,0}$ *versus* external heat flux ($\dot{q}_{ext}$ = EHF) and sample thickness (b) for PC in ASTM E1354.[27,44,45] Lines for EHF and b intersect at EHF* = 70 kW/m^2.

growth potential of polycarbonate $\lambda_{\mathrm{NRG}} = (\Delta Q/\Delta E_0)/E_{ign,0}$ is plotted in Figure 12 along with λ_{max} for polycarbonate from three laboratories.[27,44,45] There is good overall agreement between λ for the individual laboratories, with low sensitivity of λ to EHF due to the insulating and re-radiating effect of the intumescent surface char. The apparent ignition energy $E_{ign,0}$ at each b and EHF are plotted in Figure 13, showing the inverse dependence of $E_{ign,0}$ on $\dot{q}_{ext}$ suggested by equation (12).

The graphs on the left-hand side of Figure 14 are plots of $E_{ign,0}$ and λ versus b and EHF for rigid, unplasticized polyvinylchloride (PVC). The lower char fraction ($\mu = 0.19$) and smaller volumetric expansion of PVC compared with PC ($\mu = 0.24$) shows the expected
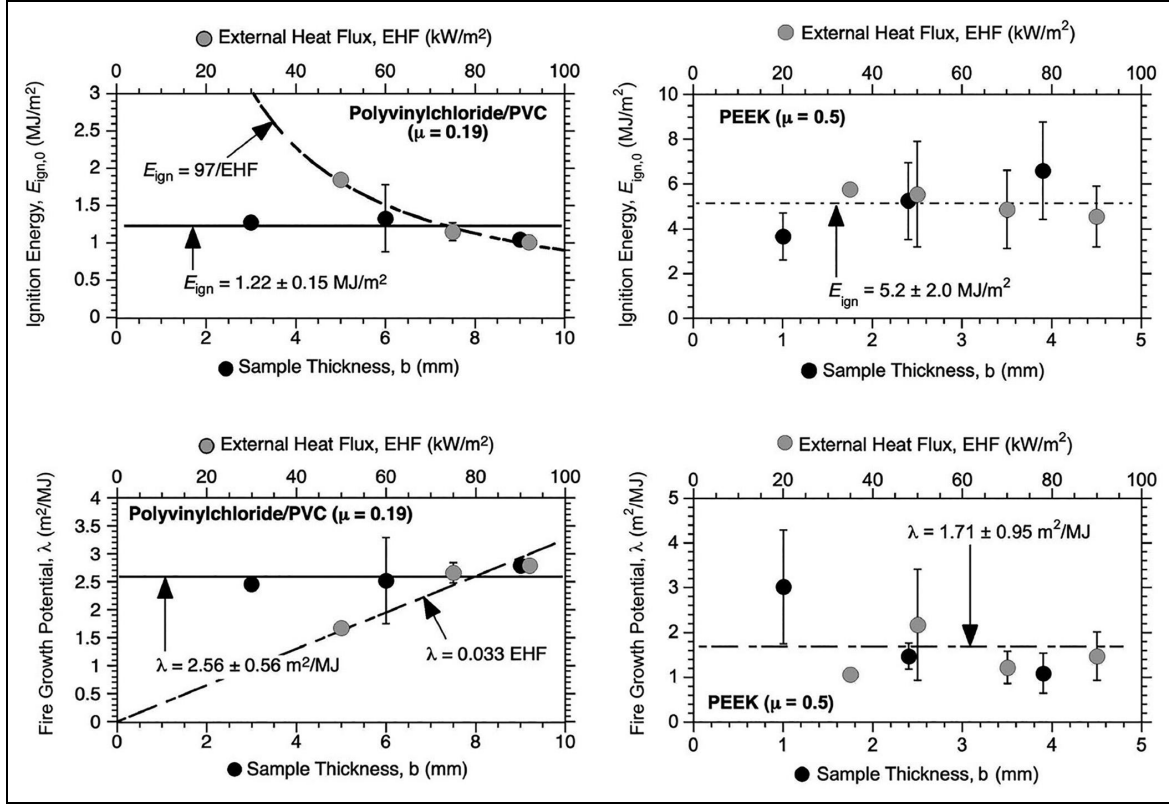
Figure 14. Nominal ignition energy $E_{ign,0}$ and fire growth potential λ of rigid polyvinylchloride/PVC and polyetheretherketone/PEEK *versus* external heat flux ($\dot{q}_{ext}$ = EHF) and sample thickness (b) in ASTM E1354. Error bars on the data points are one standard deviation of the mean with respect to the independent variable on the opposite abscissa.

independence of λ from b and linear dependence of λ on EHF as per equation (13) and the inverse relationship between $E_{ign,0}$ and EHF as per equation (12). At the crossover point, EHF* = $\dot{q}_{ext}^{*}$ = $\dot{q}_{burn}$ = 78 kW/m² = λ/K + $\dot{q}_{ign}$ (equation (23)).

The graphs on the right-hand side of Figure 14 are plots of $E_{ign,0}$ and λ versus b and EHF for polyetheretherketone/PEEK. The high char fraction (μ = 0.50) and voluminous char swelling of PEEK[46] obscures any dependence of $E_{ign,0}$ and λ on b and EHF, so the horizontal dashed lines are global averages of $E_{ign,0}$ and λ.

The $E_{ign,0}$ and λ lines in Figures 9 to 14 intersect the b lines for the non-charring polymers PMMA, HIPS, and HDPE at $\dot{q}_{ext}^{*}$ = $\dot{q}_{burn}$ = 45 ± 5 kW/m², and at $\dot{q}_{ext}^{*}$ = $\dot{q}_{burn}$ = 75 ± 5 kW/m² for the charring polymers PC and PVC. These are the external energy fluxes for burning in the cone calorimeter and they are related to the fire compliance (K) of the solid and its critical energy flux for piloted ignition $\dot{q}_{ext}^{*}$ by equation (13)

$$\dot{q}_{ext}^{*} = \dot{q}_{burn} = \frac{\lambda}{K} + \dot{q}_{ign} \qquad (23)$$

Applications

Figure 15 is a plot of λ and Π for blends of ABS with PC tested in our laboratory in triplicate as 3.2-mm thick samples at EHF = 50 kW/m² in the cone calorimeter. Both λ and Π of the
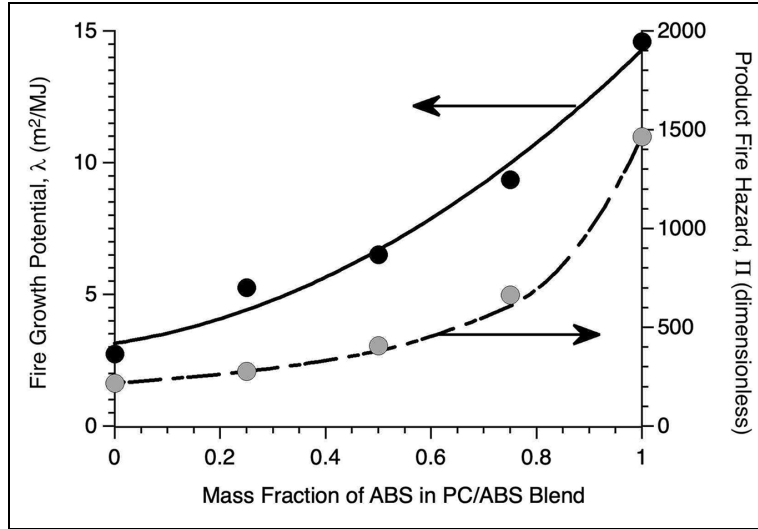
Figure 15. Fire growth potential (λ) and product fire hazard (Π) of PC/ABS blends.

blends increase monotonically according to a lower bound rule of mixtures as the mass fraction of the non-charring, more easily ignited, and higher combustibility ABS increases (compare PC and ABS in Figures 6 and 7).

Figure 16 is a plot of the material fire hazard $\pi = \Pi/b$, computed using equations (2), (3), and (21) from published cone calorimeter data. The data from Hirschler[27] are an average value of π at $\dot{q}_{ext} = 40$ and 70 kW/m^2, while π for the composites[46] are average values for the indicated resin system at an external heat flux, $\dot{q}_{ext} = 50$ kW/m^2. These π values are intensive properties that span four decades for the materials and products in Figure 16.

Figure 17 is a plot of the material fire hazard, $\pi = \Pi/b$, measured in a bench-scale (cone) calorimeter versus the molecular-scale fire hazard or fire growth capacity (FGC),[38] measured in a micro (10^{-6} kg) scale combustion calorimeter (MCC) according to ASTM D7309[39] for the pure polymers and polymer blends in Table 2 for which both values were available. Figure 17 shows that there is a high positive correlation between the bench-scale fire property π and the molecular fire property FGC, reinforcing the hypothesis that the material fire hazard π is a combustion parameter that can be measured in a cone calorimeter and used for comparison, classification, and ranking of the passive fire protection afforded by materials and products.

Figure 18 is a graphical summary of data obtained by Hong et al.[47] in a study of the effectiveness of phosphorus and bromine-containing flame-retardant additives on the fire growth of computer monitors and television sets subjected to three small open flame ignition sources for 1.5–5 minutes. The 2.1-mm thick housings for the monitor and TV were commercial products containing either NFR, a phosphorus flame retardant (PFR), or a brominated flame retardant (BFR), and were tested as free-standing, isolated articles. The housings were tested separately as rectangular bars in upward flame spread by the UL 94,[49] or downward flame spread by the limiting oxygen index (LOI).[50] Separate 10-cm square plates were tested in a cone calorimeter at $\dot{q}_{ext} = 50$ kW/m^2 according to the standard method.5 The full-scale test results for the products are plotted as binary variables in Figure 18 with $B = 0$
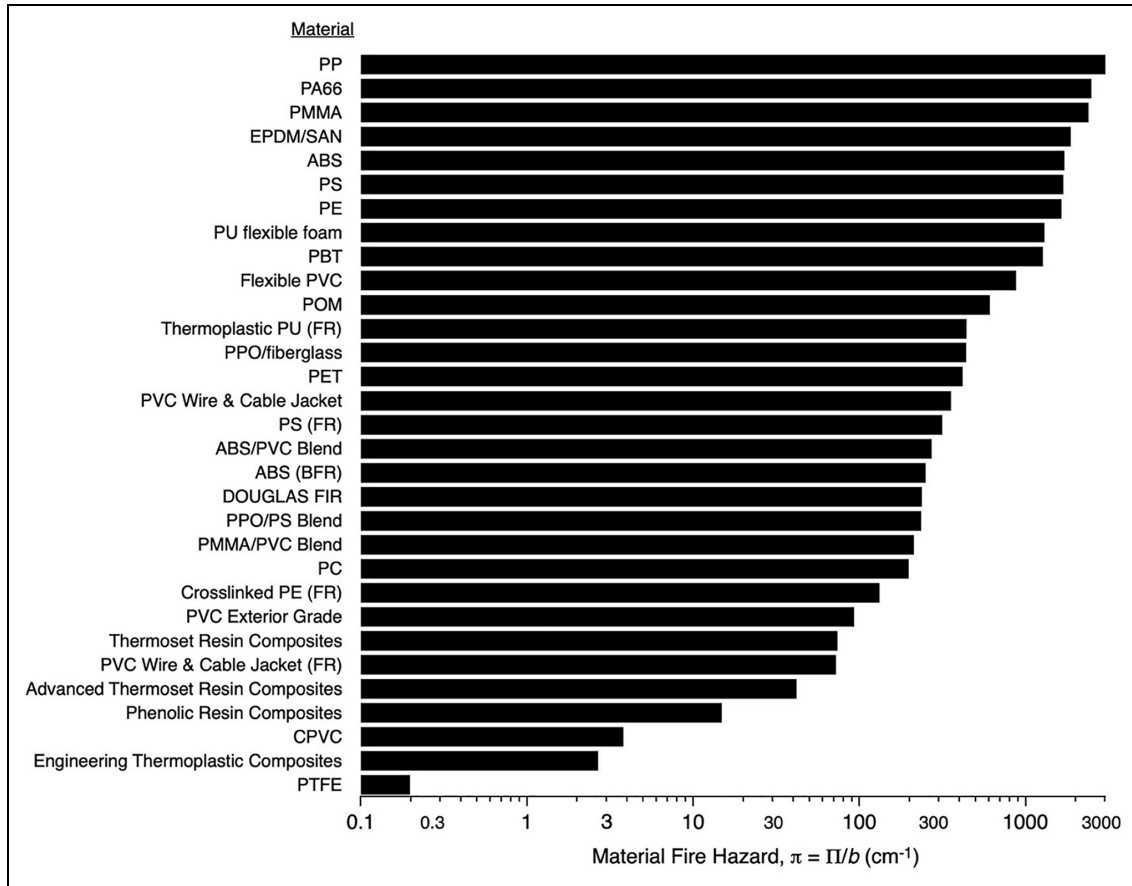
Figure 16. Material fire hazard from published cone calorimeter data.[27,46]
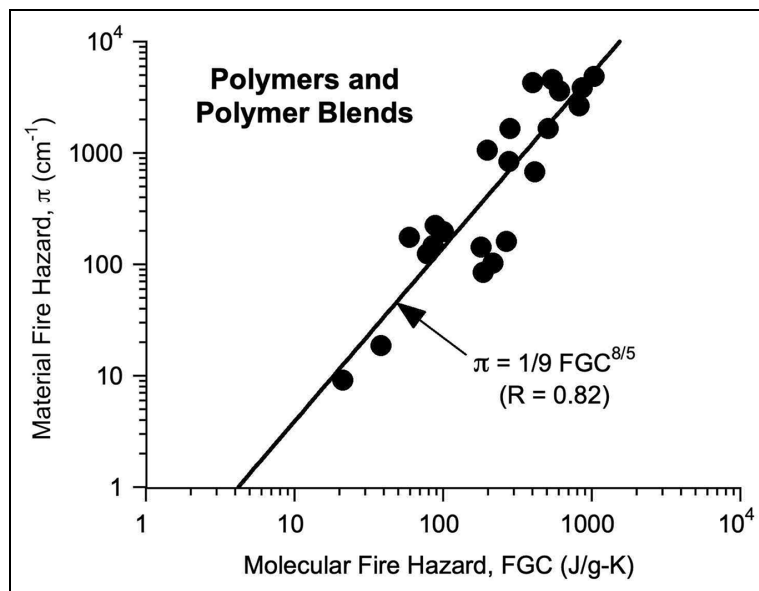

Figure 17. Bench-scale material fire hazard π (cm^{-1}) versus microscale fire growth capacity FGC (J/g-K) for 22 polymers and polymer blends. The line through data points is a power law fit having correlation coefficient R = 0.82.
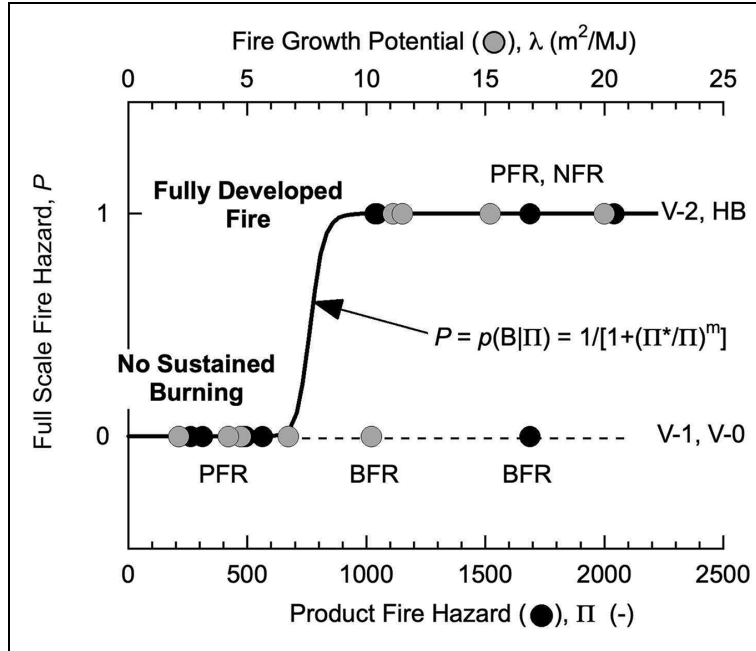
Figure 18. Results of product fire testing of computer monitors and televisions having polystyrene housings containing no flame retardant (NFR), phosphorus flame retardant (PFR), or a brominated flame retardant (BFR).[47]

corresponding to no sustained burning or $B = 1$ for a fully developed fire. These results were fit to a conditional probability function[51] with Π as the sole explanatory variable

$$P = p(B|\Pi) = \frac{1}{1 + (\Pi^{*}/\Pi)^{m}} \qquad (24)$$

Equation (24) gives the likelihood, P, that sustained burning, B, will occur in a full-scale fire test of a product having fire hazard, Π. The binary full-scale results were fit to equation (24), and the solid line in Figure 18 is the nonlinear regression line for best-fit values, $\Pi^{*} = 765$ and $m = 27$. Figure 18 indicates that computer monitors and televisions with plastic housings containing phosphorus flame retardants exhibit a loss of passive fire protection at $\Pi = 765$ or $\lambda \approx 8$ m^2/MJ, as evidenced by a rather abrupt transition at $P = \frac{1}{2}$ from no sustained burning to a fully developed fire. The UL 94 vertical flammability classifications and flame-retardant additive for the housings are indicated in Figure 18. No sustained burning is observed for V-0, V-1 classifications containing PFR or BFR additives. Fully developed fires are observed for V-2 and HB classifications containing PFR or NFR additives. These UL 94 V classifications are consistent with the IEC 62368-1 fire safety requirement for passive fire protection of plastic computer and TV housings.[52]

Figure 19 is a graphical summary of the data from a study performed at the National Institute of Standards and Technology (NIST) on the effect of flame-retardant plastic housings of computer monitors and keyboards on the full-scale fire hazard of these products.[53] The 3.2-mm thick computer housings were tested separately in a cone calorimeter at $\dot{q}_{ext} = 50$ kW/m^2 by the standard method as well as in the UL 94 vertical test of plastic flammability.[49] The products were tested as isolated, free-standing articles under a large
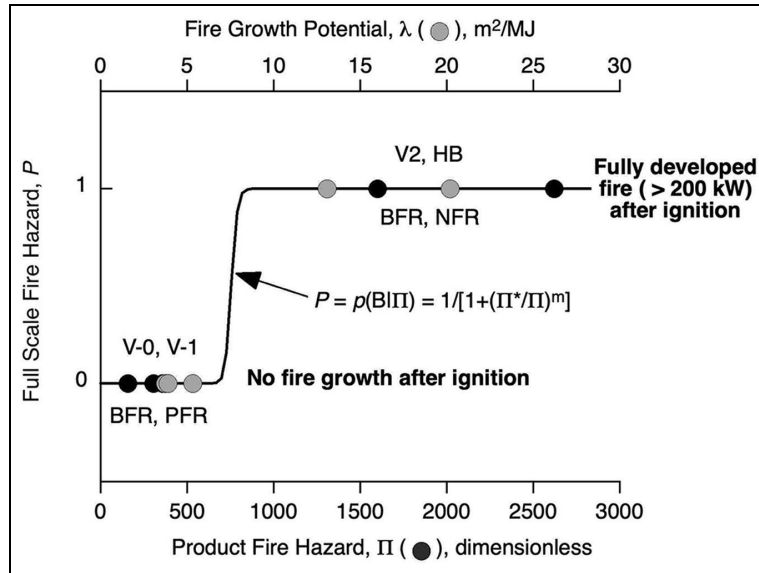
Figure 19. Results of product fire testing of computer monitors having plastic housings containing no flame retardant (NFR), phosphorus flame retardant (PFR), or a brominated flame retardant (BFR).[45,53]

hood so that heat release rate could be measured by oxygen consumption. The ignition source was a small open flame applied for 0.3, 1, or 7 minutes until burning was initiated. The binary results were reported as no sustained fire growth after ignition ($B = 0$) or a fully developed fire ($B = 1$) having a heat release rate greater than 200 kW. The solid line in Figure 19 is a fit of equation (24) to the binary full-scale data using best-fit values, $\Pi^* = 754$ and $m = 46$. The results in Figure 19 are consistent with Figure 18 in that there is no fire propagation of the free-standing monitors for flammability classifications, UL 94 V-1 and V-0, while fire growth to a fully developed fire is observed for UL 94 V-2 and HB classifications, regardless of the type of fire-retardant additive.

Figure 20 is a summary of the UL 94 vertical classifications reported in Bundy and Ohlemiller[45] and Hong et.al.,[47] versus the fire growth potential λ and product fire hazard Π computed using equations (22) and (2), respectively, from the cone calorimeter data for 1.6, 2.1, and 3.2-mm thick samples of PC, HIPS, ABS, PC/ABS, PP, and PS tested as natural materials or modified with non-halogen (mainly phosphorus) and bromine-containing flame retarding additives. The poor correlation of λ and Π with UL 94 V classifications in Figure 20 is inconsistent with the UL 94 V classification of full-scale fire growth as a categorical outcome in Figures 18 and 19 because of sample thickness, melting, dripping, and three-dimensional burning effects that influence UL 94 V classifications but have no effect on λ and Π.

Figure 21 is a plot of measured (black circles) and estimated (gray circles) times to flash-over for natural and flame-retardant wood products in the ISO 9705 room corner fire test[6] versus the product fire hazard Π computed from the published cone calorimeter data for these products.[21,22] Time to flashover in this test is defined as the time to reach a heat release rate of 1 MW in a standard 2.4 m wide × 2.4 m high × 3.6 m deep room lined with test materials on both walls and the ceiling of a corner that is ignited at the bottom with a propane burner in 10-minute sequences of 100 and 300 kW. The room fire test is used to classify
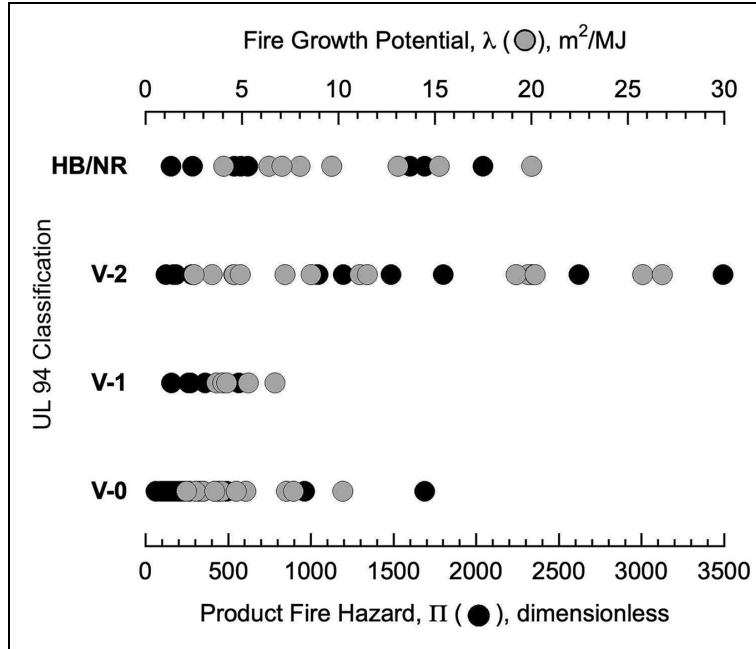
Figure 20. UL 94 V classification versus fire growth potential (λ) and product fire hazard (Π). UL and cone data from Bundy and Ohlemiller[45,53]
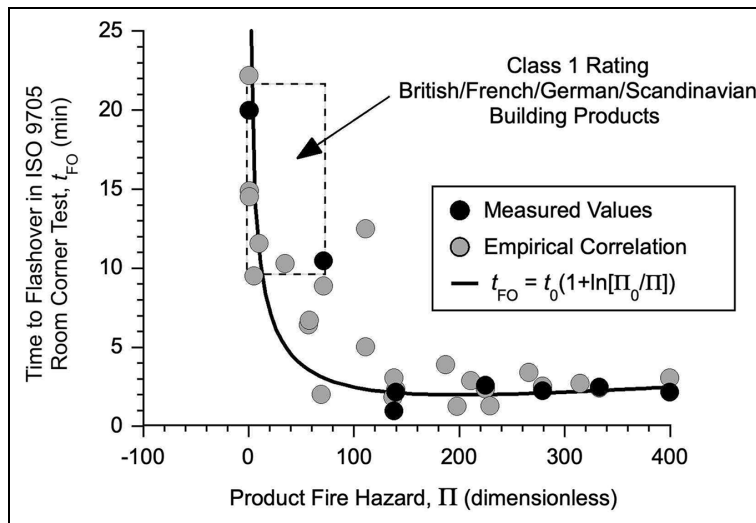

Figure 21. Time to flashover t_{FO} in the ISO 9705 room fire test versus product fire hazard Π for building products and lining materials. Solid line is fit of equation (26) to the measured data (black circles).

building products in Europe for early stage fire growth potential.[6] The empirical relationship used to estimate the times to flashover for wood and other products (gray circles) that were tested in the cone calorimeter but not in the full-scale room fire test was, $t_{FO}(s) = 0.07 t_{ign}^{0.25} \rho^{1.7}/THR^{1.3} + 60s$,[21] based on a correlation of the time to flashover in the ISO 9705 room fire test for 28 materials having density ρ and for which the time-to-ignition t_{ign} and the heat

release H_c at 300 s were measured in a cone calorimeter at $\dot{q}_{ext} = 50 \text{ kW/m}^2$ according to the standard method.[2] The trend of the measured and estimated t_{FO} versus Π shown in Figure 21 indicates that the rate of decrease in the time to flashover (1 MW) in the ISO 9705 room fire test is inversely proportional to Π, that is

$$-\frac{dt_{FO}}{d\Pi} \propto \frac{1}{\Pi} \equiv \frac{t_0}{\Pi} \tag{25}$$

Separating variables in equation (25) and integrating from the minimum value, Π_0 at flashover time t_0

$$t_{FO} = t_0 \left(1 + \ln\left[\frac{\Pi_0}{\Pi}\right] \right) \tag{26}$$

The solid line through the data points in Figure 21 is equation (26) with best-fit nonlinear regression parameters, $\Pi_0 = 200$ at $t_0 = 2$ minutes. The correlation coefficient of equation (26) to the measured t_{FO} with these parameters is $R = 0.90$. Products with $t_{FO} \geqslant 10$ minutes receive a Class 1 Rating in the British, French, German, and Scandinavian fire standards, corresponding to $\Pi \leqslant 75$ as the sole explanatory variable in Figure 21.

Summary and conclusion

The continuous and coupled processes of surface flame-spread and in-depth burning of combustible solids that drive fire growth are represented by their ignition and forced combustion behavior in a cone calorimeter as the product of ignitability and combustibility. This definition of the potential for fire growth by a combustible solid in a cone calorimeter, λ, is measured by plotting the time integral of the areal heat release rate $Q(t) = \int_0^t \dot{Q}(x)dx$ versus the time integral of the constant external energy flux $E_0(t) = \dot{q}_{ext} \int_0^t dx = \dot{q}_{ext}t$, in a combustion energy diagram of Q versus E_0 whose onset is the nominal ignition energy $E_{ign,0}$ and whose maximum slope $\Delta Q/\Delta E_0$ is the combustibility. The fire growth potential is defined by these two combustion energy diagram parameters and approximated by the parametric form

$$\lambda = Ignitability * Combustibility \equiv \left(\frac{1}{E_{ign,0}}\right)\left(\frac{\Delta Q}{\Delta E_0}\right) \approx \left(\frac{1}{\dot{q}_{ext}t_{ign}}\right)\left(\frac{\dot{Q}_{max}}{\dot{q}_{ext}}\right) \tag{27}$$

A constitutive relationship for the reaction λ of a combustible solid having fire compliance K to the thermal stress $\dot{q}_{net}$ from a heater or fire follows from steady burning and ignition theory

$$\lambda = \left(\frac{1}{\dot{q}_{net}t_{ign}}\right)\left(\frac{\dot{Q}_{ss}}{\dot{q}_{net}}\right) = \left[\frac{h_c/h_g}{\kappa\rho c_P \Delta T_{ign}^2}\right]\dot{q}_{net} = K\left(\dot{q}_{ext} - \dot{q}_{ign}\right) \tag{28}$$

The constitutive relationship equation (28) shows is that λ is proportional to the difference between $\dot{q}_{ext}$ and energy flux for ignition $\dot{q}_{ign}$. The intersection of the λ and E_{ign} lines with the

constant b lines in Figures 9 to 14 suggests that the critical energy flux for sustained burning is in the range EHF* $= \dot{q}^*_{ext} = 45 \pm 5$ kW/m^2 for non-charring materials, and $\dot{q}^*_{ext} = 75 \pm 5$ kW/m^2 for charring materials, with the value for a particular material given as

$$\dot{q}^*_{ext} = \dot{q}_{burn} = \lambda/K + \dot{q}_{ign} \tag{29}$$

Consequently, the typical literature value, $\dot{q}_{ext} = 50$ kW/m$^2 \approx \dot{q}_{burn}$ should be suitable for most non-charring polymers and considered a standard for reporting λ.

The potential of a combustible material or product to grow a fire is only realized as a hazard if the heat of combustion/fire load is sufficient to sustain fire growth. For a material or product having total heat of combustion per unit area, H_c (MJ/m^2), the dimensionless product fire hazard is

$$\Pi = \lambda H_c \tag{30}$$

The product fire hazard Π successfully correlates the categorical outcome of fire tests of free-standing telecommunication equipment (Figures 18 and 19, $\Pi = 760 \pm 8$) and the FIGRA of building materials in a full-scale ISO 9705 room fire test (Figure 21, $\Pi \approx 75$) when used as the sole explanatory variable—the critical value of which reflects the severity of the fire test. In small-scale vertical flammability tests[49,50] of thin rectangular bars, three-dimensional burning, sample thickness, and flaming drops effect the classification but have no effect on the one-dimensional, forced horizontal burning in a cone calorimeter, so the correlation of λ, Π, and π with small flame tests is expected to be, and is, poor (Figure 20). The material fire hazard, $\pi = \Pi/b$, is an intensive measure of flammability as evidenced by the successful ranking of the observed fire performance of polymers in small- and bench-scale flammability tests (Figure 16) as well as its correlation with the intensive, molecular-level, FGC of polymers (Figure 17).

ORCID iD

Richard E Lyon https://orcid.org/0000-0003-0446-8009

References

1. ASTM E906:2017. Standard test method for heat and visible smoke release rates for materials and products using a thermopile method (West Conshohocken, PA: ASTM International, 2017).
2. International Organization for Standardization (ISO) 5660-1:2002. Reaction-to-fire tests — heat release, smoke production and mass loss rate. Part 1: heat release rate (cone calorimeter method) (Geneva: ISO, 2002).
3. Code of Federal Regulations. *Title 14: aeronautics space; chapter 1: Federal Aviation Administration, Department of Transportation. Part 25*. US Government Printing Office, 2004, https://www.ecfr.gov/current/title-14/chapter-I
4. ASTM E2058:2019. Standard test methods for measurement of material flammability using a fire propagation apparatus (FPA) (West Conshohocken, PA: ASTM International, 2019).

5. ASTM E1354:2023. Standard test method for heat and visible smoke release rates for materials and products using an oxygen consumption calorimeter (West Conshohocken, PA: ASTM International, 2023).
6. International Organization for Standardization (ISO) 9705-1:2016. Full-scale room test for surface products (Geneva: ISO, 2016).
7. ASTM E2257:2022. Standard test method for room fire test of wall and ceiling materials and assemblies (West Conshohocken, PA: ASTM International, 2022).
8. NFPA 286/IBC (chapter 8 and section 803). Corner room fire test for interior wall ceiling.
9. ANSI/FM 4910-2004. American National Standard for clean room materials flammability test protocol ANSI/FM approvals 4910 (Norwood, MA: FM Approvals LLC, 2004).
10. ANSI/4880-2017. American National Standard for evaluating the fire performance of insulated building panel assemblies interior finish materials in ANSI/4880 (Norwood, MA: FM Approvals LLC, 2017).
11. Agarwal G, Wang Y, Dorofeev S, et al. Fire performance evaluation of cladding wall assemblies using the 16-ft high parallel panel test method of ANSI/FM 4880. *Fire Mater* 2021; 45: 609–623.
12. ASTM E84:2023. Standard test method for determining surface burning characteristics of building materials (Underwriters Laboratories (UL) 723) (West Conshohocken, PA: ASTM International, 2023).
13. EN 13823:2020 + A1:2022. Reaction to fire tests for building products. Building products excluding floorings exposed to the thermal attack by a single burning item.
14. McGrattan KB, McDermott RJ, Weinschenk CG, et al. *Fire dynamics simulator users guide.* Report no. 1019, 2013. Gaithersburg, MD: National Institute of Standards and Technology (NIST), https://www.nist.gov/publications/fire-dynamics-simulator-users-guide-sixth-edition
15. Stoliarov SI, Leventon IT, Lyon RE, et al. Two-dimensional model of burning for pyrolyzable solids. *Fire Mater* 2013; 38(3): 391–408.
16. Stoliarov SI and Ding Y. Pyrolysis model parameterization and fire growth prediction: the state of the art. *Fire Safety J* 2023; 140: 103905.
17. Nguyen HT, Nguyen KTQ, Le TC, et al. Review on the use of artificial intelligence to predict fire performance of construction materials and their flame retardancy. *Molecules* 2021; 26(4): 1022.
18. Numajiri F and Furukawa K. Short communication: mathematical expression of heat release rate curve and proposal of "burning index." *Fire Mater* 1998; 22: 39–42.
19. Tewarson A, Khan M, Wu PK, et al. Flammability evaluation of clean room polymeric materials for the semiconductor industry. *Fire Mater* 2001; 25: 31–42.
20. Petrella RV. The assessment of full-scale fire hazards from cone calorimeter data. *J Fire Sci* 1994; 12: 14–43.
21. Ostman BAL and Tsantaridis LD. Heat release and classification of fire retardant wood products. *Fire Mater* 1995; 19: 253–258.
22. Ostman BAL and Tsantaridis LD. Correlation between cone calorimeter data and time to flashover in the room fire test. *Fire Mater* 1994; 18: 205–209.
23. Tewarson A. Flammability parameters of materials: ignition, combustion, and fire propagation. *J Fire Sci* 1994; 12: 329–356.
24. Shields TJ, Silcock GW, Murray JJ, et al. Evaluating ignition data using the flux time product. *Fire Mater* 1994; 18: 243–254.
25. Vahabi H, Kandola BK and Saeb MR. *Flame retardancy index* for thermoplastic composites. *Polymers* 2019; 11: 407.
26. Vahabi H, Movahedifar E, Kandola BK, et al. *Flame retardancy index (FRI)* for polymer materials ranking. *Polymers* 2023; 15: 2422.
27. Hirschler MM. Heat release from plastic materials. In: Babrauskas V and Grayson SJ (eds) *Heat release in fires.* Essex: Elsevier Applied Science, 1992, pp. 207–217.
28. Hirschler MM. Analysis of heat release and other data from a series of materials tested in the cone calorimeter. In: *Proceedings of the 20th international conference on fire safety*, San Francisco, CA, 9–13 January 1995.
29. Babrauskas V. *Bench scale methods for prediction of full scale fire behavior of furnishings wall linings.* SFPE technical report 84-10, 1984. Boston, MA: Society of Fire Protection Engineers (SFPE).
30. Cleary TG and Quintiere JG. A framework for utilizing fire property tests. In: Cox G and Langford BInternational Association for Fire Safety Science (eds) *Proceedings of the 3rd international symposium on fire safety science.* New York: Elsevier Applied Science, 1991, pp. 647–656.
31. Quintiere JG and Lian D. Inherent flammability parameters—room corner test application. *Fire Mater* 2009; 33(8): 377–393.
32. Van Hees P, Hertzberg T, Steen Hansen A, et al. Development of a screening method for the SBI and room corner using the cone calorimeter. SP report 2002:11, 2002. *SP Fire Technology*, https://ri.diva-portal.org/smash/get/diva2:962225/FULLTEXT01.pdf
33. Drysdale DD. *An introduction to fire dynamics (chapters 5 and 6).* 3rd ed. West Sussex: John Wiley & Sons, Ltd, 2011.
34. Quintiere JG. *Fundamentals of fire phenomena (chapters 7 and 9).* West Sussex: John Wiley & Sons, Ltd, 2006.
35. Rasbash DJ. Theory in the evaluation of fire properties of combustible materials. In: *Proceedings of the 5th international fire protection seminar*, Karlsruhe, 22–24 September 1976, pp. 113–130.
36. Tewarson A. Heat release rate in fires. *Fire Mater* 1980; 4(4): 185–191.
37. Lyon RE. Heat release kinetics. *Fire Mater* 2000; 24: 179–186.
38. Lyon RE, Safronava N, Crowley S, et al. A molecular-level fire growth parameter. *Polym Degrad Stabil* 2021; 186: 109478.
39. ASTM D7309-23. Standard test method for determining flammability characteristics of plastics and other solid materials using microscale combustion calorimetry (West Conshohocken, PA: ASTM International, 2023).
40. Whiteley R, Elliot P, Staggs J, et al. Steady state analysis of cone calorimeter data. In: Grayson S (ed.) *Flame retardants*, vol. 7. London: Interscience, Ltd., 1996, pp. 71–78.
41. Lyon RE, Crowley S and Walters RN. Steady heat release rate by the moment–area method. *Fire Mater* 2008; 32: 199–212.
42. Lyon RE, Safronava N and Crowley S. Thermal analysis of polymer ignition. *Fire Mater* 2018; 42: 668–679.
43. Stoliarov SI, Crowley S, Lyon RE, et al. Prediction of the burning rates of non-charring polymers. *Combust Flame* 2009; 156: 1068–1083.
44. Stoliarov SI, Crowley S, Walters RN, et al. Prediction of the burning rates of charring polymers. *Combust Flame* 2010; 157: 2024–2034.
45. Bundy M and Ohlemiller T. *Bench-scale flammability measures for electronic equipment.* National Institute of Standards Technology (NIST) Interagency/Internal Report NISTIR 7031, 16 July 2003. Gaithersburg, MD: NIST.

46. Lyon RE, Balaguru PN, Foden A, et al. Fire-resistant aluminosilicate composites. *Fire Mater* 1997; 21: 67–73.
47. Hong S, Yang J, Ahn S, et al. Flame retardant performance of various UL94 classified materials exposed to external ignition sources. *Fire Mater* 2004; 28: 25–31.
48. Lyon RE and Crowley S. Fire properties of combustible materials from unsteady burning. *Fire Safety J* 2021; 120: 103054.
49. UL-94: test for flammability of plastic materials for parts in devices and appliances. Northbrook, IL: Underwriters Laboratories, Inc. (UL), 2024.
50. ASTM D2863-23. Standard test method for measuring the minimum oxygen concentration to support candle-like combustion of plastics (oxygen index) (West Conshohocken, PA: ASTM International, 2023).
51. Lyon RE and Safronava N. *A probabilistic analysis of pass/fail fire tests*. Final report DOT/FAA/TC-12/13, October 2013. Federal Aviation Administration, https://www.fire.tc.faa.gov/pdf/TC-12-13.pdf
52. International Electrotechnical Commission (IEC) 62368-1:2023. Audio/video, information and communication technology equipment —Part 1: safety requirements.
53. Bundy M and Ohlemiller T. *Full-scale flammability measures for electronic equipment*. NIST technical note 1461, August 2004. Gaithersburg, MD: National Institute of Standards and Technology (NIST).

Author biography

Richard E Lyon is a scientist/engineer with degrees in Chemical Oceanography (BS) and Polymer Science & Engineering (MS, PhD) whose career path has meandered through marine chemistry, textile chemistry, material science, composites engineering and finally, fire science of materials at the Federal Aviation Administration for the past 30+ years, during which he also managed the Fire Research Program. The author has published hundreds of journal articles and reports along the way and has received dozens of awards and several patents.